Heliyon 9 (2023) e17852

Contents lists available at ScienceDirect

Heliyon

journal homepage: www.cell.com/heliyon

lncRNA XIST inhibition promotes M2 polarization of microglial and aggravates the spinal cord injury via regulating miR-124–3p / IRF1 axis

Jin Yang, Zhiqiang Gong, Junjie Dong, Hangchuan Bi, Bing Wang, Kaili Du, Chunqiang Zhang, Lingqiang Chen *

Department of Orthopaedics, First Affiliated Hospital of Kunming Medical University, Kunming 650032, Yunnan, China

ARTICLE INFO

Keywords:
lncRNA XIST
Spinal cord injury
Microglia
Polarization
miR-124–3p
IRF1

ABSTRACT

Background: Spinal cord injury (SCI) has a high disability rate and mortality rate. Recently, LncRNA XIST has been found to be involved in the regulation of inflammatory responses. Therefore, we aimed to investigate the role of XIST in the occurrence and development of SCI and the specific regulation mechanism. **Methods**: 100 ng/mL lipopolysaccharide (LPS) was used to treat mouse microglia BV2 cells. Hitting spinal cord was performed to C57BL/6 mice for establishing SCI model. Real-time reverse transcriptase-polymerase chain reaction (RT-qPCR), Western blot, Immunofluorescence (IF) and Enzyme linked immunosorbent assay (ELISA) experiments were used to explore the function of XIST, miR-124–3p and IRF1 in LPS-induced BV2 cells. RT-qPCR, Nissl staining, IF, Western blot and ELISA experiment were performed to study the function of XIST in SCI mice. Dual-luciferase reporter assay, RNA immunoprecipitation (RIP), RT-qPCR and Western blot assays were utilized to identify the interaction among XIST, miR-124–3p and IRF1. **Results**: XIST was upregulated in LPS-induced BV2 cells and spinal cord tissues of SCI mice. Overexpression of XIST promoted the M1 microphages polarization and cytokines concentration in LPS-stimulated BV2 cells, aggravated SCI of mice. Downregulated XIST promoted M1-to-M2 conversion of microglial and relieved the injury of SCI mice. Mechanism verification indicated that XIST acted as a molecular sponge of miR-124–3p and regulated IRF1 expression. Increased miR-124–3p or reduced IRF1 inhibited M1 polarization of microglial and decreased the production of inflammatory cytokines in LPS-induced BV2 cells. Increased XIST or decreased miR-124–3p had an opposite of on LPS-induced BV2 cells. **Conclusion**: Overexpression of XIST enhanced M1 polarization of microglia and promoted the level of inflammatory cytokines through sponging miR-124–3p and regulating IRF1 expression.

1. Introduction

Spinal cord injury (SCI) is a traumatic central nervous system disease with a high incidence and unfavorable prognosis. It often leads to motor and sensory dysfunction below the injury site of patients, and seriously affects the work and life of patients. At present,

* Corresponding author. Department of Orthopaedics, The First affiliated hospital of Kunming medical University, No.295 Xichang Rd, Kunming 650032, Yunnan, China
E-mail address: chenlq@ydyy.cn (L. Chen).

https://doi.org/10.1016/j.heliyon.2023.e17852
Received 17 March 2023; Received in revised form 27 June 2023; Accepted 29 June 2023
Available online 3 July 2023

the clinical treatments of SCI mainly include surgery, medication and rehabilitation [1], but still have not achieved satisfactory results. Therefore, finding reliable therapeutic targets is crucial for treating SCI.

Microglia is a common immune cell in the central nervous system, and it is a mononuclear macrophage. Normally, microglia are in a resting state, while activated during SCI. Microglia have the ability to polarize into pro-inflammatory M1 type macrophages and anti-inflammatory M2 type macrophages [2]. M1 polarization of microglia produces pro-inflammatory cytokines TNF-α, IL-6, IL-1β and neurotoxicity factors, promotes the inflammatory response and nerve damage [3]. M2 polarization promotes the secretion of large amounts of anti-inflammatory cytokines IL-4, IL-10, and neurotrophic factors, inhibits the occurrence of inflammatory response and promotes the neuroprotective effects [4]. The research indicated that the imbalanced ratio of M1/M2 microglia might be trapped in the development process of SCI [5,6]. However, the specific mechanism of microglia polarization involved in the SCI remains unclear.

Long noncoding RNA (lncRNA) is involved in the regulation of gene expression at the transcriptional and posttranscriptional, and plays vital regulatory roles in the development process of many diseases [7–10]. Several lncRNAs had been proved to regulate the expression of downstream miRNA genes by competitively binding to miRNA through competitive endogenous RNA (ceRNA) regulatory network [8]. LncRNA X-inactive specific transcript (XIST) is widely expressed in body tissues, and related to multiple cellular physiological processes such as cell differentiation, proliferation, metastasis and apoptosis [11]. Recently, studies have found that the overexpressed XIST in the spinal cord tissue promoted the inflammatory response and neuronal apoptosis in SCI [12,13]. Zhong et al. [14] demonstrated that XIST knockdown increased the viability of microglial, repressed apoptosis and inflammation. However, the mechanism of XIST regulating microglia polarization in SCI remains unknown.

In the present study, we respectively explored the effect of XIST on microglia polarization *in vitro* and *in vivo*. At the same time, the starbase database was used to predict the downstream target genes of XIST. The results revealed that XIST acted as a ceRNA of miR-124–3p, regulated the polarization and inflammatory response of microglia in SCI by regulating IRF1. The study may provide new theoretical bases for the clinical diagnosis and treatment of SCI.

2. Methods

2.1. Experimental animals

24 female C57BL/6 mice (aged 6–8 weeks, n = 6) were purchased from Kunming Chushang technology co., ltd (Kunming, China). The mice were kept at 22 ± 1 °C with relative humidity of 45–55% and 12-h alternating light and dark. Mice were free to access food and water. All animal experiments in this study were approved by the Laboratory Animal Ethics Committee of Yunnan Laberal Biotechnology Co., Ltd (PZ20211215, 2021/12/27).

2.2. Establishment of SCI mice model

Mice were anesthetized and exposed the $T_{9\text{-}11}$ spinous process and lamina with the T_{10} lamina as the center. The T_{10} spinous process and lamina were removed. An impactor with a diameter of 1.5 mm and a weight of 3 g was used to hit the exposed spinal cord, resulting in contusion of moderate severity. Successful modeling was marked by contusion at the site of injury, convulsions in both lower extremities, and spasmodic tail motion. In the sham group, only T_{10} laminectomy was performed without impingement. One week before SCI modeling, lentivirus-encapsulated pcDNA-XIST (OV-XIST group) and sh-XIST (KD-XIST group) (synthesized by Shanghai Genepharma, China) were injected into the spinal cord of the mice, respectively.

2.3. Cell cultures and treatment

Mouse microglia BV2 were bought from COBIOER Biosciences CO., Ltd (Nanjing, China). BV2 cells were grown in RPMI-1640 medium containing 10% FBS (COBIOER, Nanjing, China). The medium was placed in a 5% CO_2 cell incubator. BV2 cells were stimulated by 100 ng/mL lipopolysaccharide (LPS) (Sigma-Aldrich, Shanghai, China) for 24 h to establish the SCI model *in vitro*.

2.4. Cell transfection

PcDNA-XIST (OV-XIST group), sh-XIST (KD-XIST group), miR-124–3p mimic, miR-124–3p inhibitor, sh-IRF1 and the corresponding negative control were synthesized by Genepharma (Shanghai, China). The above-mentioned plasmids were separately transfected into BV2 cells through Lipofectamine 3000 (Invitrogen, CA, USA). After 48 h, real-time reverse transcriptase-polymerase chain reaction (RT-qPCR) or Western blot assay was utilized to assess the efficiency of transfection.

2.5. RT-qPCR assay

The total RNA was individually extracted from spinal cord tissues and BV2 cells. Ultraviolet spectrophotometry detected the RNA integrity. cDNA was synthesized by reverse transcription of PrimeScript RT Reagent Kit (Takara, Japan). According to the instructions of SYBR Premix Ex Taq kit (Takara, Japan), the PCR reaction was performed, and the conditions were 95 °C 5 min, 95 °C for 20 s, 60 °C for 30 s and 72 °C for 20 s. A total of 40 cycles were performed. $2^{-\Delta\Delta Ct}$ method was used to calculate the relative expression level of the genes.

2.6. Western blot

The spinal cord tissue and BV2 cells were separately collected to extract the total protein using RIPA reagent (Shanghai Yeasen, China). The BCA kit (Thermo Fisher Scientific, MA, USA) determined protein concentration. Then 40 μg protein sample was taken for SDS-PAGE gel electrophoresis. The protein was then transferred to PVDF membranes (Beyotime, Shanghai China) and blocked with 5% skimmed milk. The PVDF membranes were incubated overnight with primary antibody (INOS, ARG1, IRF1, Abcam, China) at 4 °C. Secondary antibody (Abcam, China) was added after rinsing and incubated for 2 h at 37 °C. Enhanced chemiluminescence luminescent liquid (MedChem Express, China) was added to the membranes and the image was scanned by a gel imaging analyzer.

2.7. Immunofluorescence (IF) assay

The spinal cord tissues of mice were collected, embedded in paraffin and sectioned. The sections were dewaxed and subjected to antigen repair. The histochemical pen drew a circle around the tissue and an autofluorescence quencher was added. After rinsing, BSA solution (Rebiosci, Shanghai, China) was added to block the sections for 30 min.

The cells were fixed with 4% paraformaldehyde (Beyotime, Shanghai, China) and 0.3% TritonX-100 was added for transmembrane. BSA solution was added for blocking the cells at room temperature for 1 h.

The primary antibody (NEUN, IBA1, INOS, ARG1, GFAP, NF200, Abcam, China) was added and incubated overnight at 4 °C, followed by incubation with the secondary antibody (Abcam, China) at room temperature for 2 h. Rising the sections and cells with PBS, the nucleus was stained with DAPI (Sigma-Aldrich, China). Fluorescence microscope observed the results.

2.8. Enzyme linked immunosorbent assay (ELISA) assay

The concentrations of inflammatory cytokines were detected using ELISA kits (Solarbio, Beijing China). The cell culture supernatant was collected, centrifuged for 10 min at 1000 g (4 °C), and repackaged into EP tubes for storage at −20 °C. The spinal cord tissues of mice were collected and washed with PBS. The tissues were cut into pieces, PBS was added for full grinding. The homogenate was centrifuged at 5000 g for 10 min, and the supernatant was taken for detection.

The standard was diluted according to the instructions. 10 μL of sample and 40 μL of diluent was added to wells of enzyme-labeled plate. The plates were incubated at 37 °C for 30 min and washed 5 times. 50 μL of enzyme-labeled reagent was added to each well and incubated at 37 °C for 30 min. After rinsing, color developer was added for coloration. After 10 min, stop solution was added to stop the reaction. The absorbance at 450 nm was detected by microplate reader.

2.9. Nissl staining assay

The spinal cord tissues of mice were embedded in paraffin and sectioned. The sections were dewaxed and stained with 1% toluidine blue (Sigma-Aldrich, MO, USA) for 40 min. The sections were washed with distilled water, dehydrated with gradient ethanol, and treated with xylene for 5 min. Then sections were sealed with neutral glue and observed under a microscope.

2.10. Dual-luciferase reporter assay

The starbase database predicted that there were targeted binding sites between miR-124–3p and 3′ untranslated region (UTR) of XIST, IRF1. The targeting relationship was further verified by dual-luciferase reporter experiment. The wild-type (WT)/mutant (MUT) plasmid of XIST and the WT/MUT plasmid of IRF1 were transfected into BV2 cells together with NC mimic and miR-124–3p mimic, respectively. After culture for 48 h in a cell incubator, the luciferase activities were measured according to the instructions of the dual-luciferase reporter gene kit (Beyotime, Shanghai China). Renal luciferase activity was served as internal reference.

2.11. Fluorescence in situ hybridization (FISH)

The BV2 cells in logarithmic phase were digested and prepared into cell suspension, which was transferred to a Petri dish and cultured in a CO_2 cell incubator. After fixation with 200 μL anhydrous ethanol for 15 min, the samples were treated with buffer A, buffer B (RIBOBIO, Guangzhou China) and ethanol, respectively, and then incubated overnight in the mixture of probe and buffer C. The samples were washed with buffer D and stained with DAPI for 5 min. The anti-fluorescence quencher was added dropwise to Petri dish. A microscope was applied to observe and photograph.

2.12. RNA immunoprecipitation (RIP)

The RIP kit (Guangzhou Bersin Bio, China) was used to examine the interaction between XIST and miR-124–3p. The cells were fully lysed by lysate, and the supernatant was obtained by centrifugation. The lysis supernatant was mixed with magnetic bead antibody complex and incubated overnight. After RNA purification, the optical density was measured using a NanoDrop spectrophotometer (Thermo Fisher Scientific, MA, USA), and the relative levels of XIST and miR-124–3p were detected by RT-qPCR.

2.13. Statistical analysis

GraphPad Prism 8.0 was applied for statistical analyses. The data were represented as "mean ± standard deviation". Student's *t*-test was used to compare the difference between two groups. Differences among multigroup were perfumed by One-way analysis of variance, post hoc test was analyzed by Tukey's method. Two-way analysis of variance was used to compare the data with two variables. P values less than 0.05 was considered statistically significant.

3. Results

The design diagram of this study was shown in Fig. 1. First, we investigated the function of XIST in LPS-induced BV2 cells and its effect on the polarization of BV2 cells. Subsequently, the SCI model was constructed and the effect of XIST on the regulation of macrophage polarization on SCI in mice was studied *in vivo*. Using the starbase database, we further predicted the target of XIST and verified the interaction relationship between them through experiments. Finally, we explored the regulatory mechanism of XIST/miR-124–3p/IRF1 molecular axis on the polarization of LPS-induced BV2 cells.

3.1. XIST regulated the polarization of BV2 cells induced by LPS

To investigate the function of XIST in SCI, we induced BV2 cells by LPS. Results showed that the expression of XIST in BV2 cells was increased with the increase of treatment time (Fig. 2A), and the expression was highest at 24 h. Subsequently, we transfected pcDNA-XIST and sh-XIST into LPS-induced BV2 cells, respectively. RT-qPCR detection revealed that transfection of pcDNA-XIST obviously increased XIST level (Fig. 2B), and transfection of sh-XIST inhibited XIST expression.

RT-qPCR results showed that M1 macrophage markers INOS (Fig. 2C), TNF-α (Fig. 2D) and IL-1β (Fig. 2E) mRNA levels were induced by LPS, while M2 macrophage markers ARG1 (Fig. 2F), CD206 (Fig. 2G), YM1 (Fig. 2H) mRNA levels were decreased by LPS. XIST overexpression upregulated the effect of LPS on INOS, TNF-α and IL-1β mRNA, and downregulated the effect of LPS of ARG1, CD206 and YM1 mRNA. XIST inhibition had the opposite effect to XIST overexpression. Western blot (Fig. 2I–K) and IF assay (Fig. 2L–O) obtained the same results as RT-qPCR. The INOS protein (Fig. 2I and J) and fluorescence intensity (Fig. 2L-M) in LPS-induced BV2 cells was higher than PBS group, ARG1 protein (Fig. 2I and K) and fluorescence (Fig. 2N and O) in LPS-induced BV2 cells was decreased. Overexpression of XIST promoted the expression and fluorescence intensity of INOS, and inhibited ARG1. Knocking down XIST repressed INOS protein and fluorescence intensity, and enhanced ARG1 level.

ELISA kits were used to evaluated the concentration of cytokines, and revealed that treatment with LPS promoted the concentrations of pro-inflammatory cytokines TNF-α (Fig. 2P), IL-1β (Fig. 2Q) and IL-6 (Fig. 2R) in BV2 cells, and inhibited the concentration of anti-inflammatory cytokines TGF-β (Fig. 2S), IL-4 (Fig. 2T) and IL-10 (Fig. 2U). Overexpression of XIST increased the production of inflammatory cytokines and knockdown of XIST decreased the production of inflammatory cytokines in LPS-induced BV2 cells (Fig. 2P-U). These results revealed that overexpression of XIST efficiently facilitated the transformation of LPS-induced BV2 cells into M1 macrophages, downregulation of XIST promoted the of the transformation of LPS-induced BV2 cells into M2 macrophages.

3.2. XIST promoted the M1 polarization in SCI mice

We further validated the effect of XIST in SCI mice by injecting a lentivirus stably overexpression or knockdown of XIST into the spinal cord of mice. XIST was highly expressed in the spinal cord tissue of SCI mice (Fig. 3A). XIST expression was upregulated in overexpressed XIST group than in SCI group, and downregulated in knocking down XIST group. Increased XIST reduced the BMS score of mice (Fig. 3B), Nissl bodies numbers (Fig. 3C and D), inhibited the fluorescence intensity of NEUN (Fig. 3*E* and F) and NF200 (Fig. 3G and H), repressed ARG1 fluorescence intensity (Fig. 3K-L) and protein (Fig. 3M and O). INOS fluorescence intensity (Fig. 3I and J) and protein level (Fig. 3M − N) in overexpression XIST group was enhanced.

RT-qPCR and ELISA assay revealed that overexpression of XIST promoted the mRNA expression of INOS (Fig. 4A), TNF-α (Fig. 4B) and IL-1β (Fig. 4C), as well as TNF-α (Fig. 4D), IL-1β (Fig. 4E) and IL-6 (Fig. 4F) concentration. The mRNA expression of ARG1

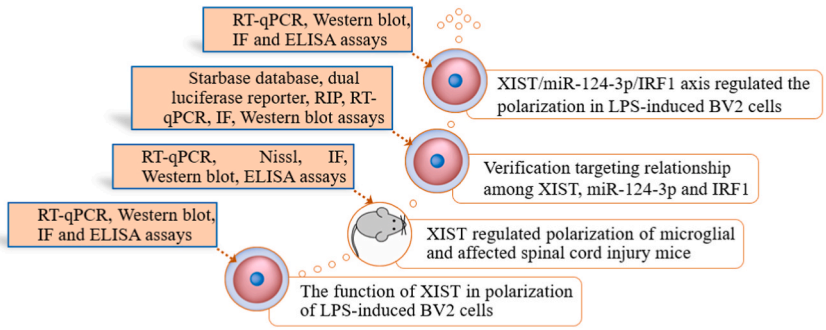

Fig. 1. Design Chart of the study.

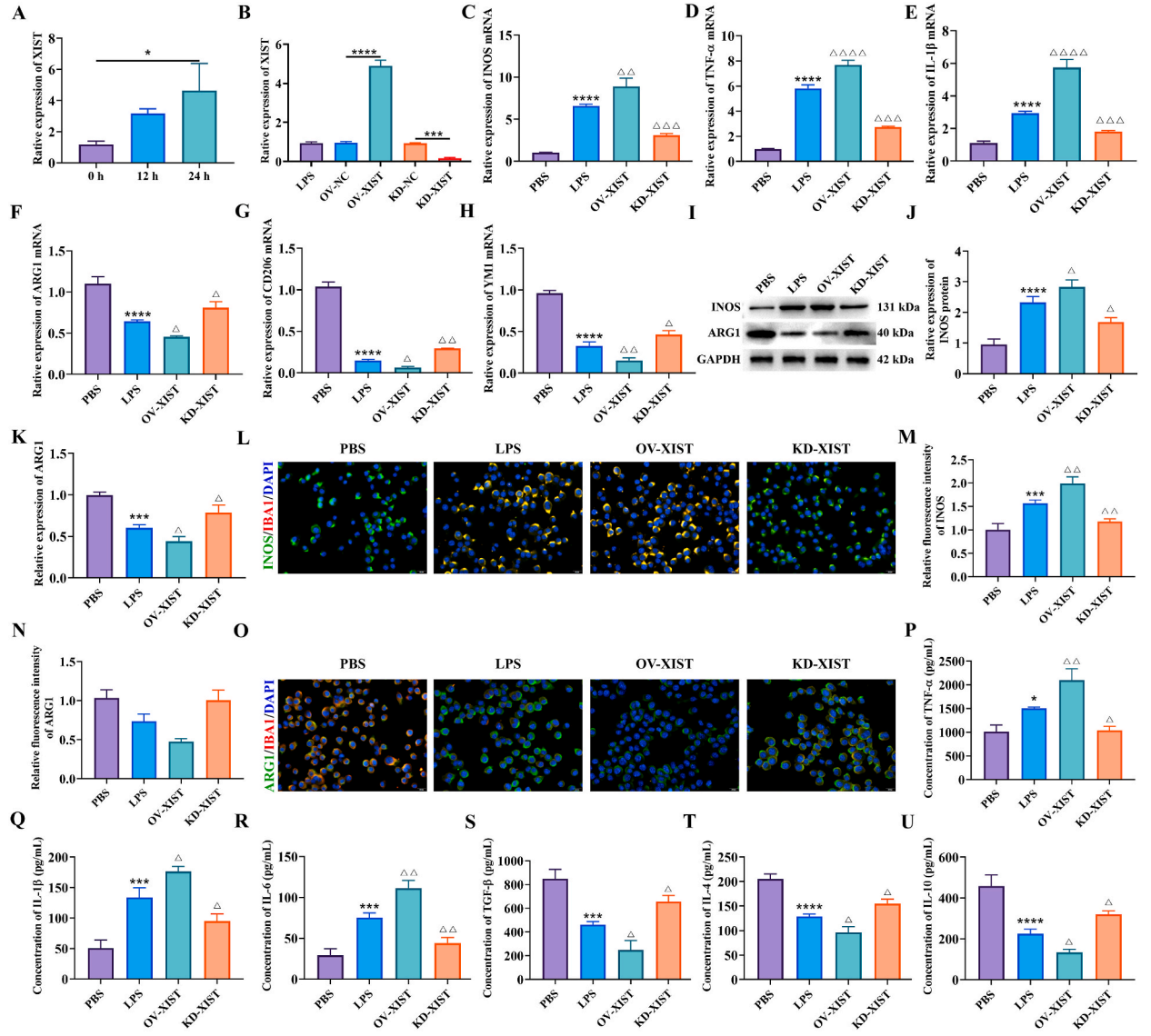

Fig. 2. XIST regulated the polarization of microglia induced by LPS.

(Fig. 4G), CD206 (Fig. 4H), YM1 (Fig. 4I) and concentrations of TGF-β (Fig. 4J), IL-4 (Fig. 4K), IL-10 (Fig. 4L) were decreased by XIST inhibition. Meanwhile, the experiments also revealed that knocking down XIST increased the BMS score of SCI mice, Nissl number, the fluorescence intensity of neuron differentiation marker gene NEUN and NF200, as well as the markers of M2 microphages, reduced concentration of inflammatory cytokines. (Fig. 3B-N, Fig. 4A-L). These experiments confirmed that overexpression of XIST aggravated SCI of mice by promoting M1 polarization of microglia, while inhibition of XIST mitigated the inflammation of SCI of mice.

3.3. XIST regulated IRF1 through sponging miR-124–3p

To further explore the downstream target genes of XIST, we predicted through starbase database and found that miR-124–3p bound with XIST (Fig. 5A), miR-124–3p had binding sites with 3′-UTR of IRF1 (Fig. 5B). Dual-luciferase assay was used to verify the interaction among XIST, miR-124–3p and IRF1. Results indicated that miR-124–3p mimic significantly decreased the luciferase activity of wild-type XIST and IRF1, while miR-124–3p mimic didn't affected the luciferase activity of mutant XIST and IRF1 (Fig. 5C and D). FISH assay showed that XIST and miR-124–3p mainly located in cytoplasm of BV2 cells (Fig. 5E). RIP results found that compared with immunoprecipitation of IgG, XIST (Fig. 5F) and miR-124–3p (Fig. 5G) visibly enriched in immunoprecipitation containing with AGO2. The further study revealed that the expression of miR-124–3p in XIST overexpression group was decreased (Fig. 5H), and upregulated in XIST inhibition group. RT-qPCR and Western blot assay verified that overexpression of miR-124–3p inhibited the mRNA (Fig. 5I) and protein (Fig. 5J) level of IRF1, while knocking down miR-124–3p upregulated IRF1 expression. In summary, XIST acted as a ceRNA

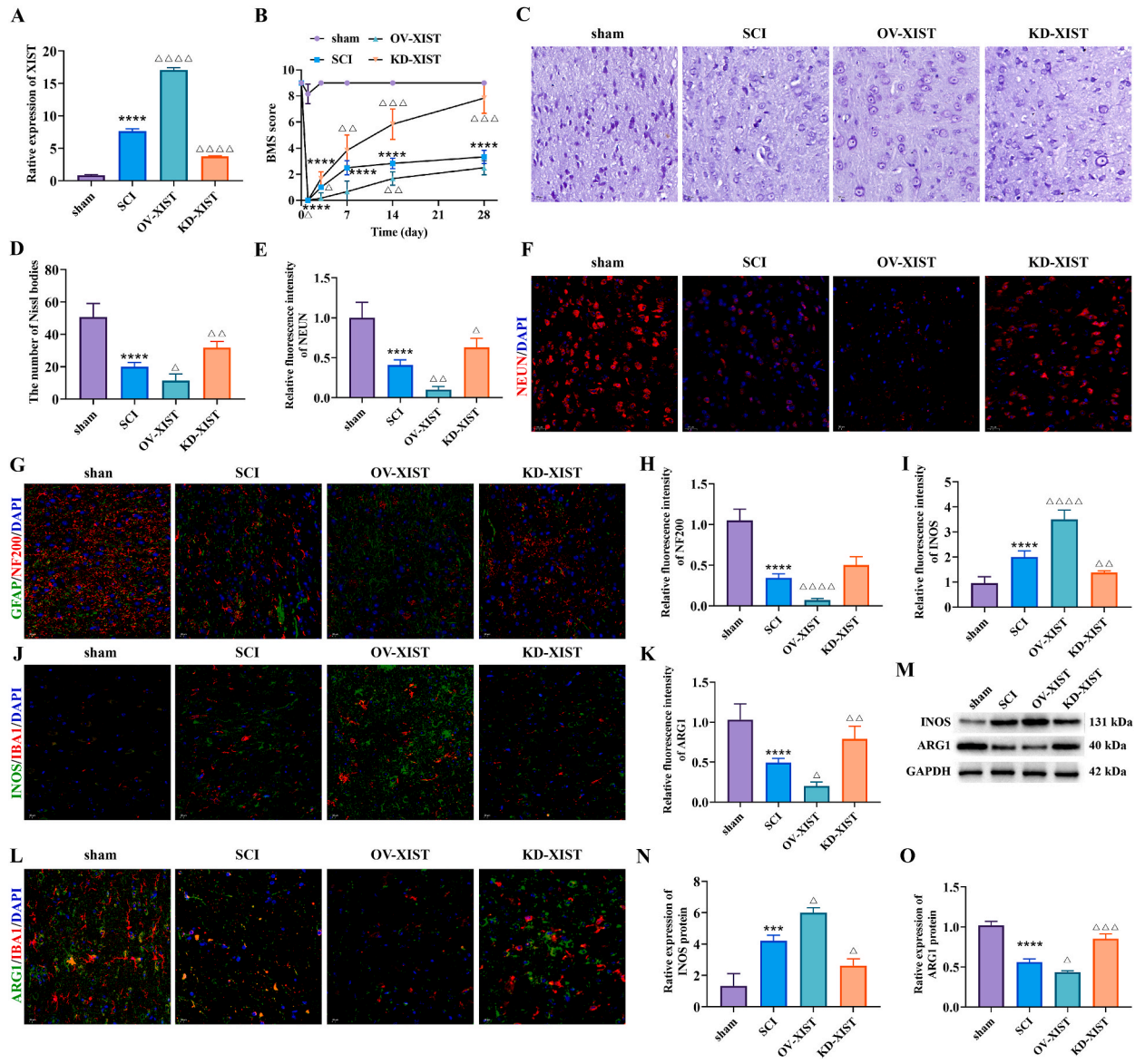

Fig. 3. XIST regulated the polarization of microglia in SCI mice.

to regulate the expression of IRF1 through sponging miR-124–3p.

3.4. XIST/miR-124–3p/IRF1 axis regulated the polarization of BV2 cells

To explore the function of XIST/miR-124–3p/IRF1 axis on LPS-induced BV2 cells. With the increase of LPS treatment time, miR-124–3p expression in BV2 cells was decreased (Fig. 6A), IRF1 protein level was increased (Fig. 6B and C). Transfection efficiency testing showed that transfection of miR-124–3p mimic significantly promoted miR-124–3p expression (Fig. 6D), transfection with miR-124–3p inhibitor decreased miR-124–3p. Transfection of sh-IRF1 inhibited IRF1 protein level (Fig. 6E and F), sh-IRF1#2 group was selected for further study.

The experiments revealed that compared with control group, increased miR-124–3p or decreased IRF1 inhibited the expression and fluorescence intensity of M1 microphage markers and increased M2 microphage markers expression and fluorescence intensity (Fig. 6G-O and Fig. 7A–D), inhibited the concentration of inflammatory cytokines (Fig. 7E–J). Overexpression of XIST or knockdown of miR-124–3p reversed the effect of increased miR-124–3p or decreased IRF1 on LPS-induced BV2 cells (Fig. 6G-O and Fig. 7A–J). These results demonstrated that overexpression of XIST promoted IRF1 expression, stimulated the transformation of LPS-stimulated BV2 cells into M1 macrophages polarization of and inflammatory cytokines concentration by sponging miR-124–3p.

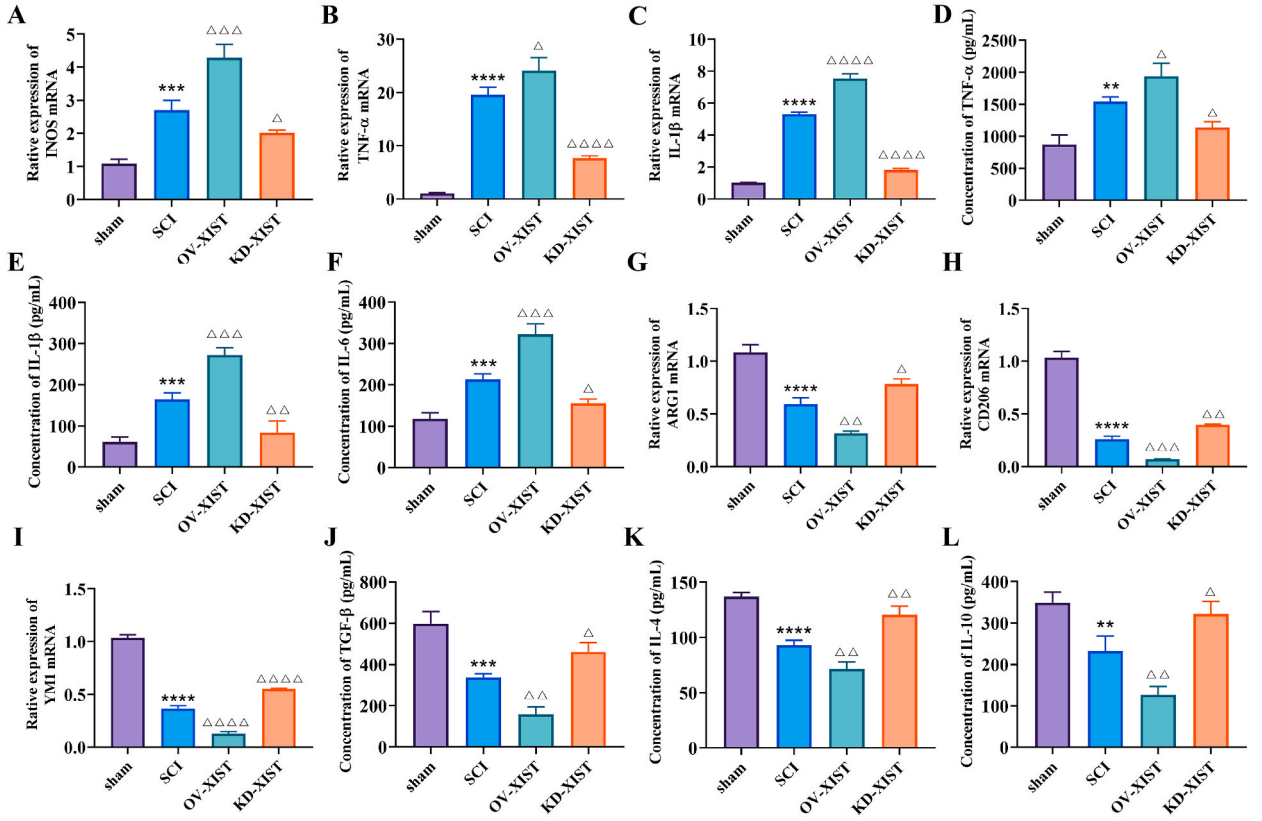

Fig. 4. XIST regulated polarization of microglia in SCI mice.

4. Discussion

SCI is usually caused by external force leading to spinal fracture, vertebral body displacement or bone fragments protruding into bone marrow. After SCI, there will be secondary injuries including neuron and nerve cell death, blood vessel rupture and blood-brain barrier destruction. The clinical symptoms of patients with SCI include spinal cord concussion, and severe patients may have high paraplegia, quadriplegia, and others may even have respiratory disorders, bladder and rectal dysfunction, etc. In recent years, the medical level has been greatly improved, but the cure rate of SCI is still low. Therefore, studying the molecular mechanism involved in regulating SCI may provide new strategies for diagnosis and treatment of SCI. Here, we found that the expression of XIST was increased in LPS-induced BV2 cells and spinal cord tissue of SCI mice, knocking down XIST promoted M2 polarization of microglial *in vitro* and *in vivo* by regulating miR-124–3p/IRF1 axis.

Microglia originates from the myeloid progenitor in the yolk sac of an embryo, which contribute to the survival and protection of neurons, as well as maintains the dynamic balance of the nervous system. It has been found that the polarization of microglia plays a key role in the development of diseases, especially in SCI [14–17]. Xue et al. [17] reported that Atractylenolide III alleviated SCI mice by promoting the transformation of M1 into M2 of microglia. Exosomes derived from periodontal ligament stem cells inhibited M1 polarization of macrophages by inhibiting the activating of ROS-MAPK-NF/kB P65 signal pathway, and promoted SCI repair [18]. We found that promoting M1 polarization of microglia in SCI mice aggravated the injury in SCI mice, while promoting M2 polarization of microglia alleviated on the injury of SCI mice through repressing inflammation response.

Recent reports showed that the abnormal expression of lncRNAs was closely related to the occurrence of SCI [19,20]. For example, knocking down lncRNA NEAT1 reduced the lesions in the spinal cord of SCI mice and the number of cavities in the damaged spinal cord and weakens neuronal apoptosis by upregulating the expression of miR-29b [21]. Silencing of lncRNA GBP9 promoted M2 polarization in macrophages and facilitated the injury repair in SCI rats [22]. LncRNA Vof-16 was upregulated after SCI, and inhibition of lncRNA Vof-16 contributed to nerve regeneration and functional repair after SCI in rats [23]. Overexpression of lncRNA FTX woke the inflammatory reaction of microglia induced by LPS, which was beneficial to the injury repair of SCI rats [24]. In the study, XIST expression was elevated in SCI tissues and LPS-induced BV2 cells. Overexpressed XIST promoted M1 polarization of BV2 cells and the production of inflammatory cytokines, aggravated neural damage in SCI mice. Downregulation of XIST promoted M2 polarization of BV2 cells and promoted neural repair in SCI mice. Moreover, XIST has also been found to be involved in the regulation of polarization in other microphages. Zhao et al. [11] found that decreased XIST induced M1-to-M2 microphages-type conversion to promoted cell proliferation and migration of breast cancer. Upregulated XIST promoted polarization of M2 microphages in lung cancer [25]. XIST

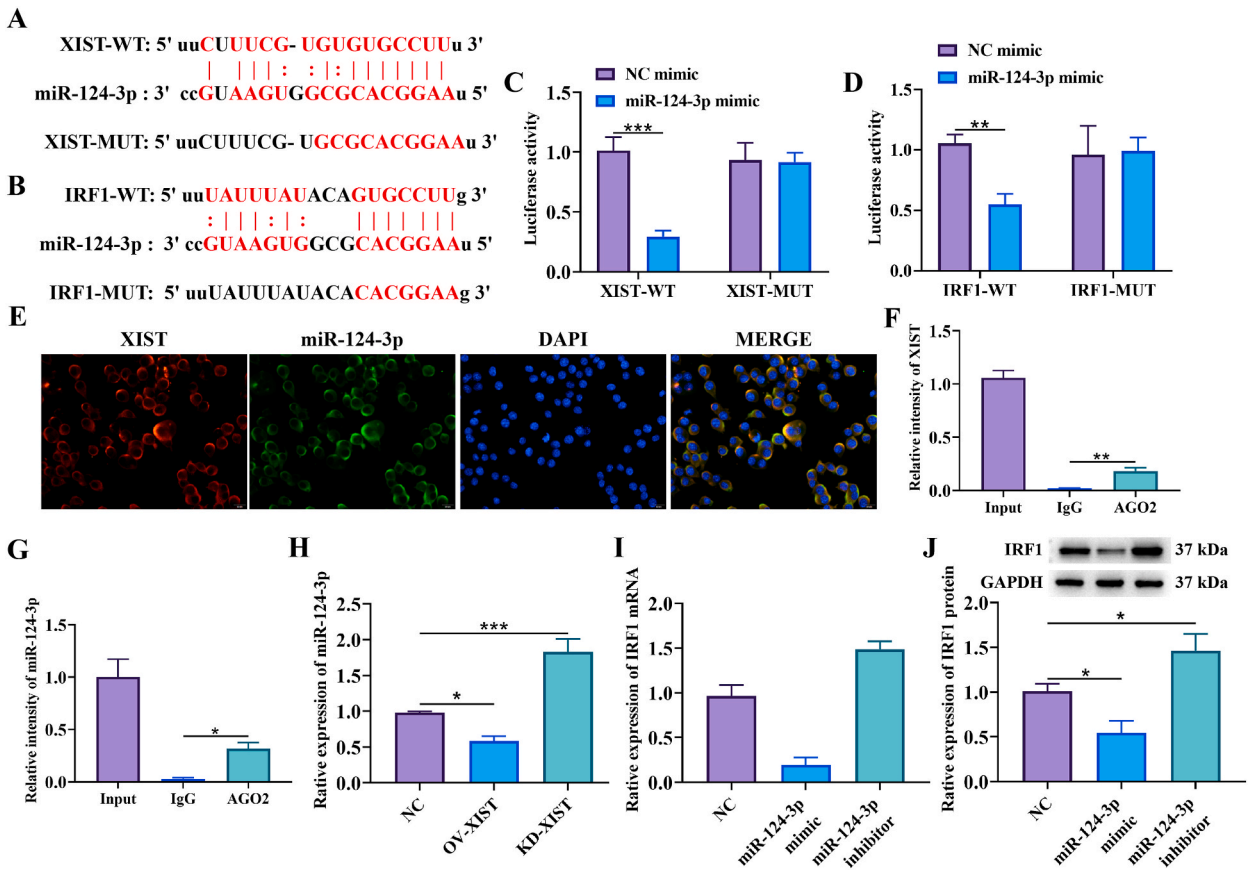

Fig. 5. XIST regulated IRF1 through sponging miR-124–3p.

enhanced fibroblast extracellular matrix production by promoting the transformation of microphages to M2 phenotype [26]. Machine learning is an auxiliary tool commonly used to predict diseases recently. Artificial neural network is one of machine learning algorithms, which is constantly optimized in the process of application [27,28]. Based on machine learning, Parodi et al. [29] found that XIST was overexpressed in women and non-relapsed Hodgkin's lymphoma, which may be the reason for the favorable prognosis of female patients with Hodgkin's lymphoma. More functions of XIST in diseases need to be explored and discovered by people using machine learning.

miRNA is an important regulator of SCI [30,31]. For example, anti-inflammatory microglia exosome-derived miR-672–5p promoted the functional behavior recovery of mice with traumatic SCI by inhibiting neuronal apoptosis [32]. miR-487 b inhibited inflammation and neuronal apoptosis in LPS-induced BV2 cells and SCI rats [33]. In this study, we found that miR-124–3p was a target of XIST. Overexpression of miR-124–3p inhibited LPS-induced M1 polarization of BV2 cells and the concentration of inflammatory cytokines, promoted the generation of anti-inflammatory cytokines. At the same time, we proved that IRF1 was a potential target of miR-124–3p, and overexpressed miR-124–3p significantly inhibited the expression of IRF1. In addition, miR-124–3p has also been reported to inhibit inflammatory reactions in other diseases such as allergic rhinitis [34], acute kidney injury caused by ischemia-reperfusion [35] and osteoarthritis [36].

IRF1 is a member of interferon regulatory factor family, acts as an activator of innate and acquired immune responses, and participates in the regulation of host response to viral and bacterial infections, cell proliferation, apoptosis, and the immune response [37,38]. For instance, IRF1 promoted the innate immune response to viral infection by promoting the activation of IRF3 [39]. Inhibition of IRF1accelarated the polarization of M2 macrophages in glioblastoma cells and increased tumor infiltration [40]. Knocking down IRF1 alleviated the injury of SH-SY5Y cells induced by oxygen and glucose deprivation and reoxygenation [41]. In this study, we proved that IRF1 in LPS-induced BV2 cells was overexpressed, and knocking down IRF1 significantly inhibited M1 polarization of BV2 cells and upregulated the level of anti-inflammatory factors.

In conclusion, we clarified for the first time that overexpression of XIST upregulated promoted M1 polarization and inflammation response of BV2 cells, exacerbated the nerve damage of SCI mice (Fig. 8). XIST inhibition, miR-124–3p overexpression or IRF1 inhibition promoted the M2 polarization of BV2 cells and decreased cytokines concentration, as well as mitigated the injury of SCI mice. Mechanism study indicated XIST sponged miR-124–3p and regulated IRF1 expression. The XIST/miR-124–3p/IRF1 axis may provide a potential therapeutic target for SCI. However, there are still some shortcomings in this study. The downstream signaling pathway regulated by IRF1 remains unclear and needs to be further explored.

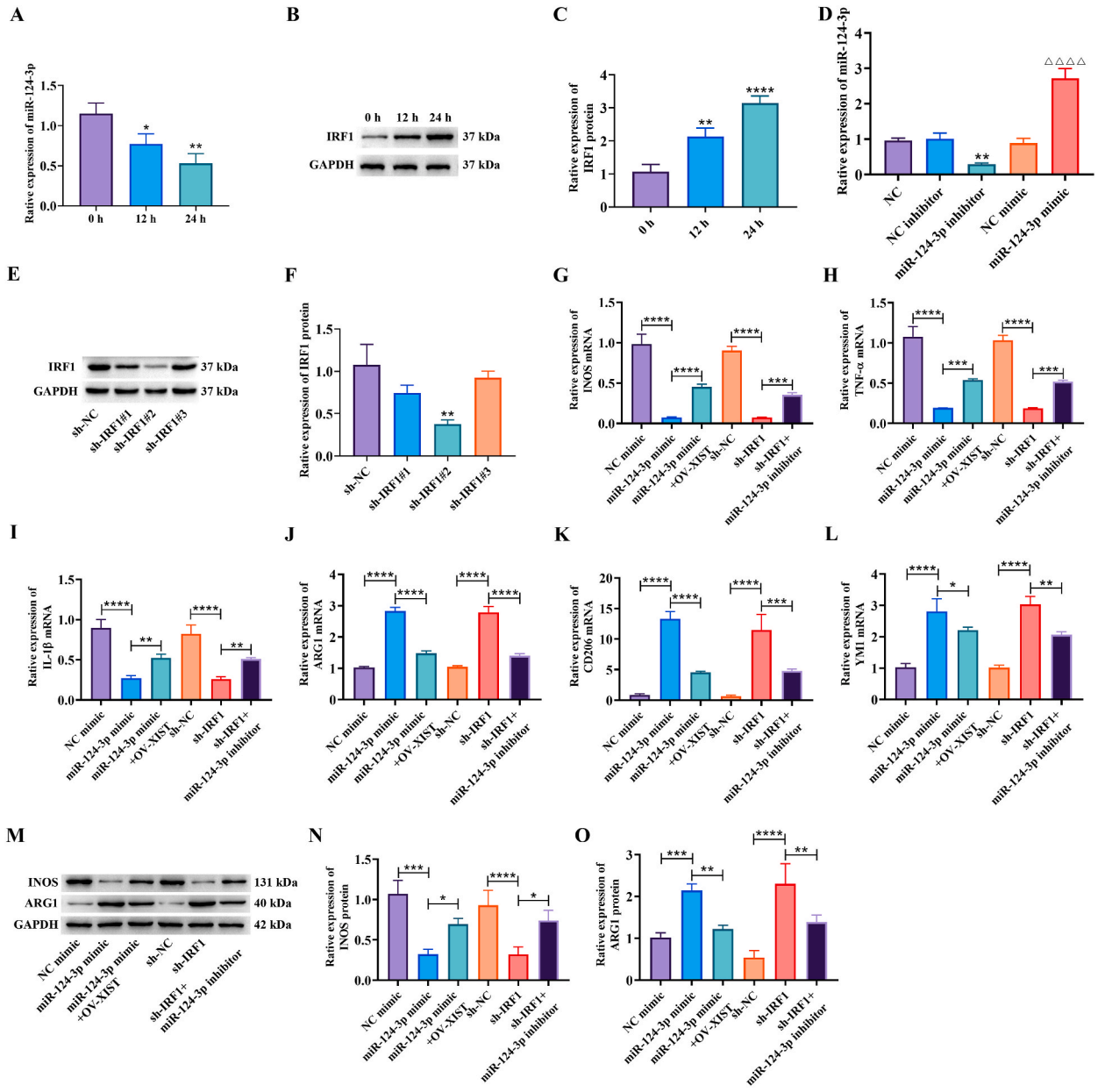

Fig. 6. XIST/miR-124–3p/IRF1 axis regulated the polarization of LPS-induced BV2 cells.

Declarations

Ethics statement

This study was approved by the Laboratory Animal Ethics Committee of Yunnan Laberal Biotechnology Co., Ltd (PZ20211215, 2021/12/27).

Author contribution statement

Jin Yang, Zhiqiang Gong, Lingqiang Chen: Conceived and designed the experiments; Contributed reagents, materials, analysis tools or data. </p>

Junjie Dong, Hangchuan Bi, Bing Wang: Performed the experiments. </p>

Kaili Du, Chunqiang Zhang: Analyzed and interpreted the data; Wrote the paper. </p>

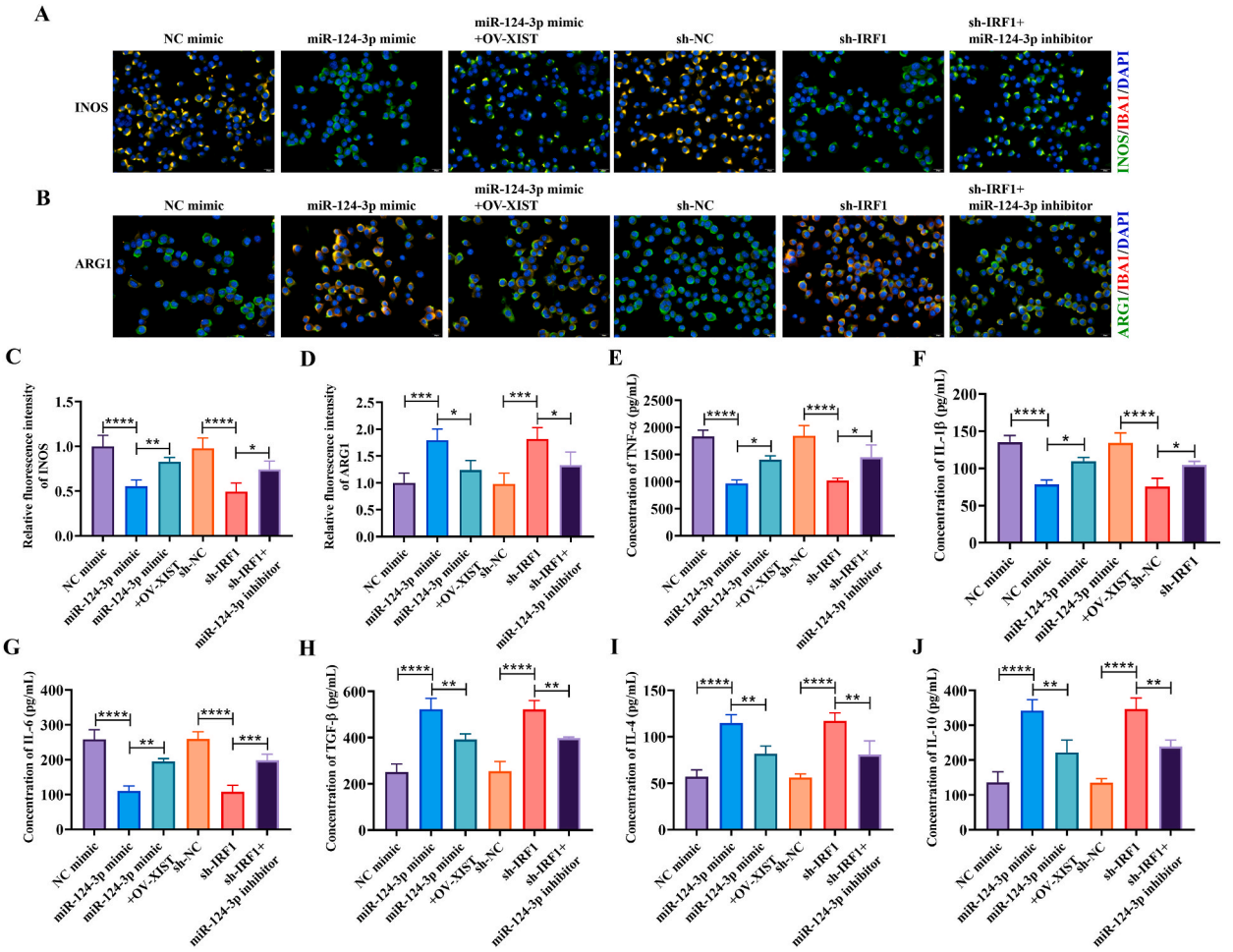

Fig. 7. XIST/miR-124–3p/IRF1 axis regulated the polarization of LPS-induced BV2 cells.

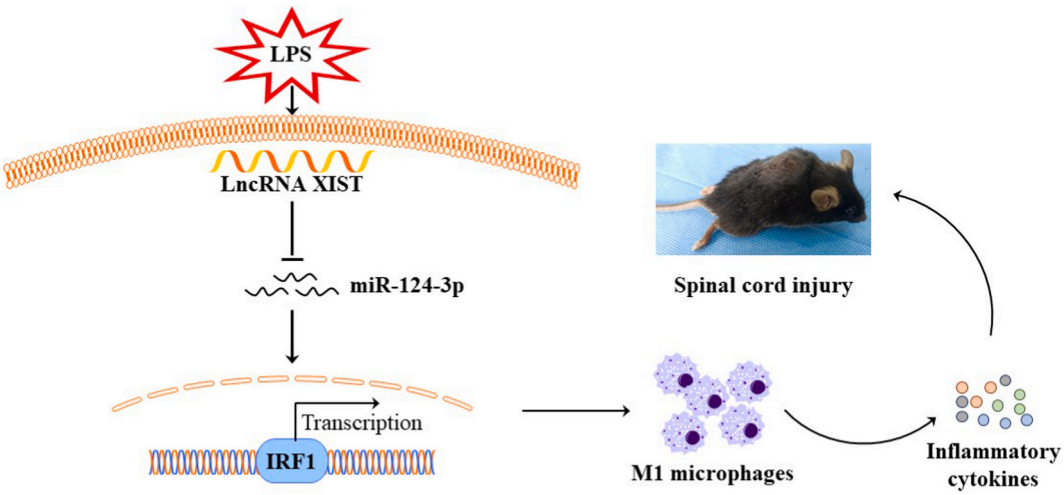

Fig. 8. XIST/miR-124–3p/IRF1 regulated polarization of microglial and modulated the SCI of mice.

Funding statement

Dr Lingqiang Chen was supported by Project of Yunnan Province Science & Technology Department Basic Research for Application (202101AT070226), National Natural Science Foundation of China (NSFC) (81860093 and 81660215), Distinguished Youth Cultivation Program of Associated Project of Yunnan Province Science & Technology Department and Kunming Medical University Basic Research for Application (202101AY070001-031), Associated Project of Yunnan Province Science & Technology Department and Kunming Medical University Basic Research for Application ((2019FE001(-207)) and Sub project of special fund of Yunnan orthopedics and sports rehabilitation clinical medicine research center (202102AA100068).

Data availability statement

Data included in article/supp. Material/referenced in article.

Declaration of competing interest

The authors declare no known conflicts of interest.
Appendix A Supplementary data to this article can be found.

Appendix A. Supplementary data

The following is the Supplementary data to this article.

Appendix B. Supplementary data

Supplementary data to this article can be found online at https://doi.org/10.1016/j.heliyon.2023.e17852.

A. RT-qPCR was applied to detect XIST expression. B. RT-qPCR detected the efficiency of transfection. Compared with 0 h group, $^{*}P < 0.05$, $^{***}P < 0.001$, $^{****}P < 0.0001$. RT-qPCR (*C*–H), Western blot (I–K) and IF (L-O, 40 ×) assays were perfumed to assess the expression of microphage markers. *P*–U. ELISA kit assessed the concentration of cytokines. Compared with PBS group, $^{*}P < 0.05$, $^{***}P < 0.001$, $^{****}P < 0.0001$. Compared with LPS group, $^{\triangle}P < 0.05$, $^{\triangle\triangle}P < 0.01$, $^{\triangle\triangle\triangle}<0.001$, $^{\triangle\triangle\triangle\triangle}P < 0.0001$.

A. RT-qPCR assessed the level of XIST. B. BMS score of mice. C and D. Nissl staining of spinal cord tissues (40 ×). IF assay was performed to detected the fluorescence intensity of NEUN (E-F), GFAP and NF200 (G-H), INOS (I-J) and ARG1 (K-L) (40 ×). M-O. Western blot detected INOS and ARG1 protein. Compared with PBS group, $^{***}P < 0.001$, $^{****}P < 0.0001$. Compared with LPS group, $^{\triangle}P < 0.05$, $^{\triangle\triangle}P < 0.01$, $^{\triangle\triangle\triangle}<0.001$, $^{\triangle\triangle\triangle\triangle}P < 0.0001$.

A-C and G-I. RT-qPCR measured the mRNA expression of microphage markers. D-F and J-L. ELISA kit assessed the concentration of cytokines. Compared with PBS group, $^{**}P < 0.01$, $^{***}P < 0.001$, $^{****}P < 0.0001$. Compared with LPS group, $^{\triangle}P < 0.05$, $^{\triangle\triangle}P < 0.01$, $^{\triangle\triangle\triangle}<0.001$, $^{\triangle\triangle\triangle\triangle}P < 0.0001$.

A. Starbase database predicted the binding sequences among XIST, miR-124–3p and IRF1. C and D. Dual luciferase reporter gene assay verified the interaction among XIST, miR-124–3p and IRF1. E. The location of XIST and miR-124–3p in BV2 cells was performed by FISH assay (40 ×). F and G. AGO2-RIP assay was applied to determine XIST and miR-124–3p enrichment in immunoprecipitated. H and I. RT-qPCR assessed the expression of miR-124–3p and IRF1 mRNA. J. The protein level of IRF1 was measured by Western blot. $^{*}P < 0.05$, $^{**}P < 0.01$, $^{***}P < 0.001$.

A. RT-qPCR detected miR-124–3p expression. B and C. Western lot was used to detect IRF1 protein. D. RT-qPCR was performed to assess miR-124–3p expression. E and F. IRF1 protein was detected using Western blot. G-L. The mRNA expression of microphage markers was measured by RT-qPCR. M-O. Western blot assessed the protein level of INOS and ARG1. $^{*}P < 0.05$, $^{**}P < 0.01$, $^{***}P < 0.001$, $^{****}P < 0.0001$.

A-D. IF assay measured the fluorescence intensity of microphage markers (40 ×). *E*-J. ELISA kit assessed the concentration of cytokines. $^{*}P < 0.05$, $^{**}P < 0.01$, $^{***}P < 0.001$, $^{****}P < 0.0001$.

Schematic diagrams revealed that increased XIST enhanced IRF1 expression through sponging miR-124–3p, accelerated the phenotypic transformation of microglia into macrophage M1 and the production of inflammatory cytokines, which aggravated the spinal cord injury (SCI) in mice.

References

[1] M. Karsy, G. Hawryluk, Modern medical management of spinal cord injury[J], Curr. Neurol. Neurosci. Rep. 19 (9) (2019) 65.
[2] B. Fan, Z. Wei, X. Yao, et al., Microenvironment imbalance of spinal cord injury[J], Cell Transplant. 27 (6) (2018) 853–866.
[3] X. Ma, S. Wang, C. Li, et al., Baicalein inhibits the polarization of microglia/macrophages to the M1 phenotype by targeting STAT1 in EAE mice[J], Int. Immunopharm. 113 (Pt A) (2022), 109373.
[4] J. Deng, F. Meng, K. Zhang, et al., Emerging roles of microglia depletion in the treatment of spinal cord injury, J. Cell. 11 (12) (2022).
[5] H. Fan, H.B. Tang, Z. Chen, et al., Inhibiting HMGB1-RAGE axis prevents pro-inflammatory macrophages/microglia polarization and affords neuroprotection after spinal cord injury[J], J. Neuroinflammation 17 (1) (2020) 295.

[6] T. Kuboyama, S. Kominato, M. Nagumo, et al., Recovery from spinal cord injury via M2 microglial polarization induced by Polygalae Radix[J], Phytomedicine 82 (2021), 153452.
[7] Y. Zhang, S. Guo, S. Wang, et al., LncRNA OIP5-AS1 inhibits ferroptosis in prostate cancer with long-term cadmium exposure through miR-128-3p/SLC7A11 signaling[J], Ecotoxicol. Environ. Saf. 220 (2021), 112376.
[8] K. Guo, K. Qian, Y. Shi, et al., LncRNA-MIAT promotes thyroid cancer progression and function as ceRNA to target EZH2 by sponging miR-150-5p[J], Cell Death Dis. 12 (12) (2021) 1097.
[9] X. Meng, Y. Zhang, Y. Hu, et al., LncRNA CCAT1 sponges miR-218-5p to promote EMT, cellular migration and invasion of retinoblastoma by targeting MTF2[J], Cell. Signal. 86 (2021), 110088.
[10] Y.T. Tan, J.F. Lin, T. Li, et al., LncRNA-mediated posttranslational modifications and reprogramming of energy metabolism in cancer[J], Cancer Commun. 41 (2) (2021) 109–120.
[11] Y. Zhao, Z. Yu, R. Ma, et al., lncRNA-Xist/miR-101-3p/KLF6/C/EBPα axis promotes TAM polarization to regulate cancer cell proliferation and migration[J], Mol. Ther. Nucleic Acids 23 (2021) 536–551.
[12] X. Cheng, J. Xu, Z. Yu, et al., LncRNA xist contributes to endogenous neurological repair after chronic compressive spinal cord injury by promoting angiogenesis through the miR-32-5p/notch-1 Axis[J], Front. Cell Dev. Biol. 8 (2020) 744.
[13] S. Gu, R. Xie, X. Liu, et al., Long coding RNA XIST contributes to neuronal apoptosis through the downregulation of AKT phosphorylation and is negatively regulated by miR-494 in rat spinal cord injury[J], Int. J. Mol. Sci. 18 (4) (2017).
[14] X. Zhong, Y. Bao, Q. Wu, et al., Long noncoding RNA XIST knockdown relieves the injury of microglia cells after spinal cord injury by sponging miR-219-5p[J], Open Med. 16 (1) (2021) 1090–1100.
[15] X. Lan, X. Han, Q. Li, et al., Modulators of microglial activation and polarization after intracerebral haemorrhage[J], Nat. Rev. Neurol. 13 (7) (2017) 420–433.
[16] Z. Yin, Z. Han, T. Hu, et al., Neuron-derived exosomes with high miR-21-5p expression promoted polarization of M1 microglia in culture[J], Brain Behav. Immun. 83 (2020) 270–282.
[17] M.T. Xue, W.J. Sheng, X. Song, et al., Atractylenolide III ameliorates spinal cord injury in rats by modulating microglial/macrophage polarization[J], CNS Neurosci. Ther. 28 (7) (2022) 1059–1071.
[18] C. Liu, F. Hu, G. Jiao, et al., Dental pulp stem cell-derived exosomes suppress M1 macrophage polarization through the ROS-MAPK-NFκB P65 signaling pathway after spinal cord injury[J], J. Nanobiotechnol. 20 (1) (2022) 65.
[19] X. Li, Y. Qian, K. Tang, et al., Inhibition of lncRNA H19/miR-370-3p pathway mitigates neuronal apoptosis in an in vitro model of spinal cord injury (SCI)[J], Transl. Neurosci. 12 (1) (2021) 103–113.
[20] C. Guan, Y. Wang, LncRNA CASC9 attenuates lactate dehydrogenase-mediated oxidative stress and inflammation in spinal cord injury via sponging miR-383-5p [J], Inflammation 44 (3) (2021) 923–933.
[21] G. Bai, L. Jiang, P. Meng, et al., LncRNA Neat1 promotes regeneration after spinal cord injury by targeting miR-29b[J], J. Mol. Neurosci. 71 (6) (2021) 1174–1184.
[22] J. Zhou, Z. Li, T. Wu, et al., LncGBP9/miR-34a axis drives macrophages toward a phenotype conducive for spinal cord injury repair via STAT1/STAT6 and SOCS3[J], J. Neuroinflammation 17 (1) (2020) 134.
[23] X.M. Zhang, L.N. Zeng, W.Y. Yang, et al., Inhibition of LncRNA Vof-16 expression promotes nerve regeneration and functional recovery after spinal cord injury [J], Neural Regen Res 17 (1) (2022) 217–227.
[24] W. Xiang, L. Jiang, Y. Zhou, et al., The lncRNA Ftx/miR-382-5p/Nrg1 axis improves the inflammation response of microglia and spinal cord injury repair[J], Neurochem. Int. 143 (2021), 104929.
[25] Y. Sun, J. Xu, TCF-4 regulated lncRNA-XIST promotes M2 polarization of macrophages and is associated with lung cancer[J], OncoTargets Ther. 12 (2019) 8055–8062.
[26] L. Pi, B. Fang, X. Meng, et al., LncRNA XIST accelerates burn wound healing by promoting M2 macrophage polarization through targeting IL-33 via miR-19b[J], Cell Death Dis. 8 (1) (2022) 220.
[27] Y. Gao, H. Liu, X. Wang, et al., On an articial neural network for inverse scattering problems[J], J. Comput. Phys. 448 (2022), 110771.
[28] W. Yin, W. Yang, H. Liu, A neural network scheme for recovering scattering obstacles with limited, phaseless far-field data[J] 417 (2020), 109594.
[29] S. Parodi, C. Manneschi, D. Verda, et al., Logic Learning Machine and standard supervised methods for Hodgkin's lymphoma prognosis using gene expression data and clinical variables[J], Health Inf. J. 24 (1) (2018) 54–65.
[30] W. Liu, Y. Rong, J. Wang, et al., Exosome-shuttled miR-216a-5p from hypoxic preconditioned mesenchymal stem cells repair traumatic spinal cord injury by shifting microglial M1/M2 polarization[J], J. Neuroinflammation 17 (1) (2020) 47.
[31] Y. Zhang, T. Meng, J. Chen, et al., miR-21a-5p promotes inflammation following traumatic spinal cord injury through upregulation of neurotoxic reactive astrocyte (A1) polarization by inhibiting the CNTF/STAT3/Nkrf pathway[J], Int. J. Biol. Sci. 17 (11) (2021) 2795–2810.
[32] Z. Zhou, C. Li, T. Bao, et al., Exosome-Shuttled miR-672-5p from anti-inflammatory microglia repair traumatic spinal cord injury by inhibiting AIM2/ASC/Caspase-1 signaling pathway mediated neuronal pyroptosis[J], J. Neurotrauma 39 (15–16) (2022) 1057–1074.
[33] D. Tong, Y. Zhao, Y. Tang, et al., MiR-487b suppressed inflammation and neuronal apoptosis in spinal cord injury by targeted Ifitm3[J], Metab. Brain Dis. 37 (7) (2022) 2405–2415.
[34] Q. Liu, Y. Shen, Y. Xiao, et al., Increased miR-124-3p alleviates type 2 inflammatory response in allergic rhinitis via IL-4Rα[J], Inflamm. Res. 71 (10–11) (2022) 1271–1282.
[35] Q. Xue, L. Yang, H. Wang, et al., Silence of long noncoding RNA SNHG14 alleviates ischemia/reperfusion-induced acute kidney injury by regulating miR-124-3p/MMP2 Axis[J], BioMed Res. Int. 2021 (2021), 8884438.
[36] B. Wang, J. Li, F. Tian, Downregulation of lncRNA SNHG14 attenuates osteoarthritis by inhibiting FSTL-1 mediated NLRP3 and TLR4/NF-κB pathway through miR-124-3p[J], Life Sci. 270 (2021), 119143.
[37] H. Feng, Y.B. Zhang, J.F. Gui, et al., Interferon regulatory factor 1 (IRF1) and anti-pathogen innate immune responses[J], PLoS Pathog. 17 (1) (2021), e1009220.
[38] H. Zhou, Y.D. Tang, C. Zheng, Revisiting IRF1-mediated antiviral innate immunity[J], Cytokine Growth Factor Rev. 64 (2022) 1–6.
[39] J. Wang, H. Li, B. Xue, et al., IRF1 promotes the innate immune response to viral infection by enhancing the activation of IRF3[J], J. Virol. 94 (22) (2020).
[40] Y. Shi, B. Zhang, J. Zhu, et al., miR-106b-5p inhibits IRF1/IFN-β signaling to promote M2 macrophage polarization of glioblastoma[J], OncoTargets Ther. 13 (2020) 7479–7492.
[41] Z.D. Liu, Q. Wang, D.Q. Pan, et al., MicroRNA-130b inhibits cerebral ischemia/reperfusion induced cell apoptosis via regulation of IRF1[J], Eur. Rev. Med. Pharmacol. Sci. 24 (23) (2020) 12334–12341.